ISSN: 3066-8131
Research Article

Science Set Journal of Physics

Start-off MHD Electroosmotic Couette Flow in an Annulus Filled with a Porous Material: A Semi-analytical Method

Michael O Oni[1], Basant K Jha[1], Baba I Mundi[3], Junaid M Abba[3], and Olaife H Adebayo[1]

[1]*Department of Mathematics, Ahmadu Bello University, Zaria, Nigeria*
[3]*Nigerian Institute of Transport Technology, NITT, Zaria, Nigeria*

***Corresponding author:** Michael O Oni, Department of Mathematics, Ahmadu Bello University, Zaria, Nigeria.

Submitted: 12 June 2024 **Accepted:** 18 June 2024 **Published:** 25 June 2024

https://doi.org/10.63620/MKSSJP.2024.1038

Citation: *Oni, M. O., Jha, B. K., Mundi, B. I., Abba, J. M., & Adebayo, O. H. (2024). Start-off MHD Electroosmotic Couette Flow in an Annulus Filled with a Porous Material: A Semi-analytical Method. Sci Set J of Physics, 3(3), 01-10.*

Abstract

The time dependent Couette flow (CF) of a conducting fluid formed between two concentric tubes filled with a porous material with variable electric potential and interplay of motion of the outer/inner cylinders is investigated. The governing electric field potential as well as the momentum equivalences are gotten from Poisson–Boltzmann and Navier Stokes equations respectively. As a promising tool for solving time-dependent problems, the Laplace-transform technique is employed to get analytical solution for velocity profile in Laplace realm. By employing the Riemann sum approximation (RSA) simulation, the results are obtained numerically in time-domain. During the graphical and numerical simulation of obtained results, it is found that the magnitude of electrokinetic effect as well as Debye-Hückel parameter play important role in flow formation and mass flow rate in the horizontal annulus. Furthermore, motion of the cylinders can serve as control mechanisms to lower or enhance mass flow rate and skin friction.

Keywords: Electroosmotic Flow (EOF), Unsteady, Couette Flow, Annuli, MHD.

Nomenclature

- c_0 concentration of ions in bulk fluid
- B magnetic field induction vector
- B_0 magnetic field strength
- $E_{z'}$ electrostatic intensity
- F Faraday's constant
- g acceleration due to gravity
- G dimensionless parameter
- J current density vector
- m' positive integer
- M Hartmann number
- LT Laplace transform
- R' universal gas constant
- r_1 radius of inner cylinder
- r_2 radius of outer cylinder
- r dimensional radial coordinate
- R dimensionless radial coordinate
- t dimensionless time
- T temperature of the fluid
- u dimensional velocity
- u' constant reference velocity
- U dimensionless velocity
- v vectorial velocity profile
- z valence number of ions in the solution
- z' axial coordinate
- η dimensional time
- ε fluid permittivity
- ζ_r ζ_2/ζ_1 (dimensionless)
- ζ zeta- potential (electrokinetic potential of the wall in the double layer)
- ϕ electrostatic potential
- Φ externally imposed electrostatic potential
- κ Debye-Huckel parameter
- λ_D Debye length
- λ annular gap (λ=r_2/r_1)
- ψ' dimensional EDL potential
- ψ dimensionless EDL potential
- μ fluid dynamic viscosity

- ρ fluid density
- σ electrical conductivity of the fluid
- τ skin friction
- ν kinematic viscosity
- ρ_f fluid density
- ρ_e charge density

Subscripts

- 1 value at the surface r=r_1
- λ value at the surface r=r_2

Introduction

Electroosmotic flow refers to the study of electrically driven mechanical motion of charged particles or fluid. This phenomenon was first observed by Reuss in 1808, in the electrophoresis of clay particles [1]. This study continues to gain attention owing to its applications in water supply, medical science and electro-mechanical devices. One of the most significant applications is the design of micropumping devices used in drug delivery, fuel supply and biochemical reactive platform [2]. Generally, an electric double-layer (EDL) is induced when solid surfaces which usually acquire a negative electric charge comes in contact with a fluid containing dissociated salt [3, 4]. This interaction generates an electric force near the wall, thereby provoking fluid motion, which subsequently transmitted to the bulk fluid by viscous forces [5].

It is well-known that the basic factors controlling the flowrate in electroosmotic pumping are: the strength of the externally applied electric field, the cross-sectional dimensions of the annulus, the microchannel surface charge density and the ion density/PH of the working fluid [6]. Although increasing the magnitude of externally applied electric field enhances flowrate, but this can cause a huge increase in the temperature of the fluid and as a result increasing the Joule heating effect, which is not advantageous [4]. Therefore, other mechanism must be used to achieve high volume flow rate. A lot of efforts and research both theoretically and experimentally have been conducted to solve the aforementioned problem [7-13]. Most of which have used pulsating force as a control mechanism for flowrate.

The study of magnetohydrodynamics in annular geometry has rapidly become a research field due to its technological applications, such as drilling operation of oil and gas wells. By assuming that the magnetic lines of forces are fixed relative to the fluid, Katagiri investigated the Couette flow formation of viscous, incompressible and electrically conducting fluid between two-infinite parallel plane walls subjected to transversely applied magnetic field and found that skin friction increases with increase in Hartmann number [14]. Later, Muhuri extended the problem by imposing a uniform suction velocity on the walls and obtained that skin friction is enhanced by increasing suction parameter [15]. Singh and Kumar on the other hand considered the same problem by assuming that the magnetic lines of force are fixed relative to the moving plate for both the impulsive and motion of the moving plates and concluded that the effect of magnetic field is to increase fluid velocity for both cases [16].

In annular geometry, the study of electrically conducting fluid was first carried out by Globe [17]. Ever since then, different articles have been credited to capture a more physical phenomena [18-22]. Jha and Apere, investigated the unsteady MHD Couette flow in an annulus by using the Riemann-sum approximation technique to obtain the results from Laplace domain to time domain [22]. They deduced that skin friction is a decreasing function of Hartmann number at the outer surface of the inner cylinder. Also, they did not analyse the role of magnetic field as well as accelerated motion of the boundary on volumetric flow-rate. Other recent related articles on electroosmotic flow and magnetic field can be seen in [23, 24].

The novelty of the current work is the development of mathematical models to theoretically analyse the unsteady electrokinetic Couette flow in a horizontal annulus filled with electrically conducting fluid with a porous material. One real-world application of this configuration can be found in the design and optimization of certain types of electromagnetic pumps. These pumps utilize the principles of MHD to move electrically conducting fluids, such as liquid metals or molten salts, without the need for any moving mechanical parts. Another physical application of start-up flow can be seen during the ignition of a rocket engine, the start-up flow plays a vital role in establishing the necessary conditions for efficient combustion and thrust generation. This entire article can be viewed as an extension of by incorporating the electrokinetic effect due to its applications in micropumping devices [22]. Further, we intend to investigate the role of magnetic field in transverse direction as well as motion of the cylinder surface on volumetric flow-rate and skin-frition, so as to serve as a control mechanism. The governing equations as well as the analytical solutions are presented in section two while the discussion of results and conclusions respectively follow in subsequent sections.

Mathematical Construction

A time dependent, fully developed, laminar flow of conducting fluid between two concentric tubes with variable electric potential is considered. The radiuses of the inside and outside cylinders are assumed to be r_1 and r_2 respectively. The inner cylinder and outer cylinder are assumed to be to move with uniform velocity A and B respctively. The flow is driven by combined external voltage gradient and motion of the cylinders. Electric potential ζ_1,ζ_2 such that $\zeta\_2>\zeta\_1$ are applied on the surface of the inner tube and outer cylinder respectively (see Fig. 1). The EDL follows Boltzmann distribution, so that the convection due to ion effects are insignificant. Also, the wall potentials are assumed small, so that Debye-Huckel linearization to be useable. All other physical thermodynamics parameters are assumed constant.

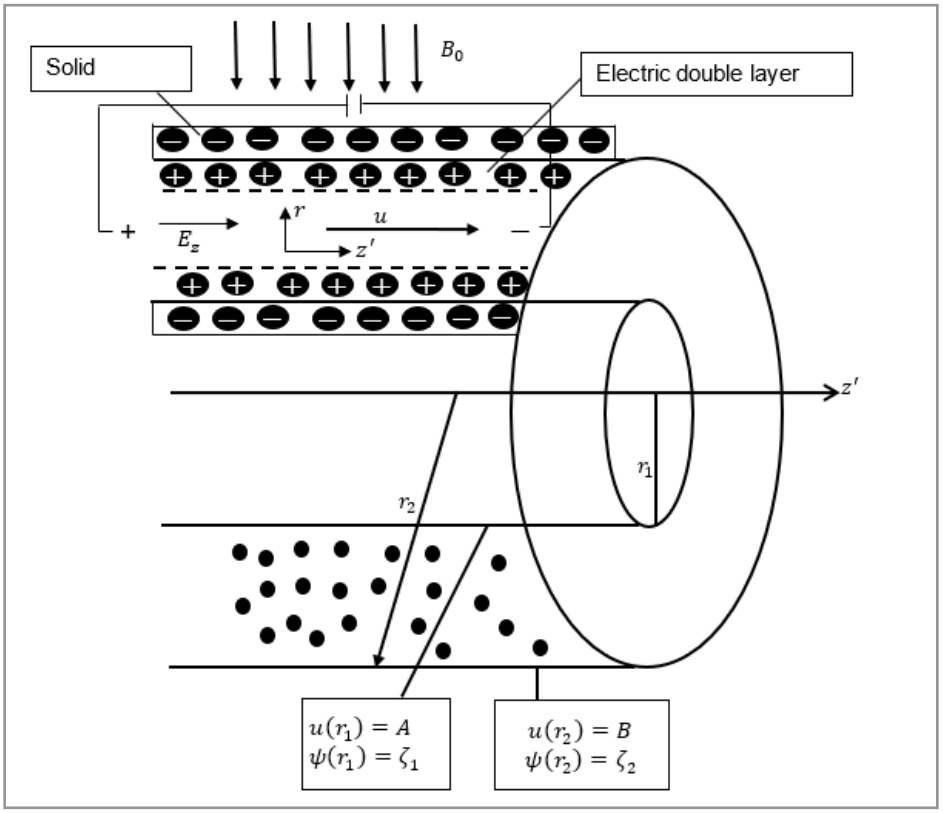

Figure 1: Schematic diagram of the problem

Electric Field Potential

Following assumptions above, the electrical potential is obtained as:

$$\nabla^2\phi = -\frac{\rho_e}{\varepsilon} \tag{2.1}$$

The potential, ϕ is due to combination of externally forced field Φ and EDL potential ψ^'. Where ρ_e is the net volume charge density of symmetric electrolyte and defined as [3]

$$\rho_e = -2FzC_0 \sinh\left(\frac{zF\psi'}{R'T}\right); \nabla = \frac{\partial}{\partial r}\vec{i} + \frac{1}{r}\frac{\partial}{\partial\phi}\vec{j} + \frac{\partial}{\partial z'}\vec{k} \tag{2.2}$$

For fully developed flow, the external potential gradient is in the axial direction only ϕ=ϕ(r) and ψ'=ψ' (r)

$$\left[\frac{1}{r}\frac{\partial}{\partial r}\left(r\frac{\partial\psi'}{\partial r}\right)\right] = \frac{2FzC_0}{\varepsilon}\sinh\left(\frac{zF\psi'}{R'T}\right) \tag{2.3}$$

subject to the boundary condition:

$$\psi'(r_1) = \zeta_1\,, \psi'(r_2) = \zeta_2, \tag{2.4}$$

where ζ_1,ζ_2 are zeta-potential at the surfaces of the cylinders Since the wall potential are assumed low enough for Debye-Huckel linearization to be valid, equations (2.3) and (2.4) in dimensionless form become [12]:

$$\frac{d^2\psi}{dR^2} + \frac{1}{R}\frac{d\psi}{dR} - \kappa^2\psi = 0\,. \tag{2.5}$$

$$\psi(1) = \zeta_r, \psi(\lambda) = 1, \tag{2.6}$$

Velocity Profile

The momentum equation governing the flow formation of an electrically conducting fluid in a horizontal concentric cylinder is obtained from the Navier-Stokes equation in vectorial form as [20]:

$$\rho_f\left(\frac{\partial v}{\partial t} + (v\cdot\nabla)v\right) = -\nabla p + \mu\nabla^2 v + \rho_e E_{z'} + JXB \tag{2.7}$$

Considering a time dependent magnetohydrodynamically fully developed flow in a concentric annulus, the above equation reduces to:

$$\frac{\partial u}{\partial\eta} = \nu_{eff}\left(\frac{\partial^2 u}{\partial r^2} + \frac{1}{r}\frac{\partial u}{\partial r}\right) - \frac{\sigma B_0^2}{\rho}u - \frac{\nu u}{K} + \varepsilon\left(\frac{d^2\psi'}{dr^2} + \frac{1}{r}\frac{d\psi'}{dr}\right)E_{z'}, \tag{2.8}$$

subject to the following initial and boundary conditions:

$$u(r,0) = 0, \quad u(r_1,\eta) = A, \quad u(r_2,\eta) = B, \tag{2.9}$$

where ν is the kinematic viscosity, K is the porosity of the porous material, and A,B are constants which assume 0 and 1 for different physical situations as follows:

5. The paragraph before (2.10) “where m’ is appositive interger…” should be completely removed.
6. Equations (2.12) and (2.13) should be corrected as:

$$\begin{cases} \text{CASE I } A=1, B=1 & \text{motion of both cylinders} \\ \text{CASE II } A=1, B=0 & \text{motion of the inner cylinder only} \\ \text{CASE III } A=0, B=1 & \text{motion of the outer cylinder only} \\ \text{CASE IV } A=0, B=0 & \text{static cylinders} \end{cases} \tag{2.10}$$

Using the following dimensionless parameters on equations (2.8) and (2.9), we have [3, 4, 22]:

$$R=\frac{r}{r_1},\ U=\frac{uv}{u' r_1^2},\ M^2=\frac{\sigma B_0^2 r_1^2}{v\rho},\ t=\frac{\eta v}{r_1^2},\ \lambda=\frac{r_2}{r_1},\ \zeta_r=\frac{\zeta_1}{\zeta_2}$$

$$\left[\frac{\varepsilon R' T}{2F^2 Z^2 C_0}\right]^{1/2}, G=\frac{2F^2 Z^2 C_0 r_1^2}{R' T u'} E_{z'},\ Da=\frac{K}{r_1^2},\ \gamma=\frac{v_{eff}}{v}. \tag{2.11}$$

$$\frac{1}{\gamma}\frac{\partial U}{\partial t}=\left(\frac{\partial^2 U}{\partial R^2}+\frac{1}{R}\frac{\partial U}{\partial R}\right)-\left[\frac{M^2 Da+1}{\gamma Da}\right]U+\frac{1}{\gamma}G\psi, \tag{2.12}$$

subject to:

$$U(R,0)=0,\quad U(1,t)=A,\quad U(\lambda,t)=B, \tag{2.13}$$

Mathematical Solution of the Problem

It is important to note that the electric potential equation is obtained from the Poison equation and therefore only the steady state solution is possible. Hence the solution of (2.5 and 2.6) is obtained as:

7. In equation (2.14), $\psi(R)$ is missing i.e $\psi(R)=C_1 I_0(\kappa R)+C_2 K_0(\kappa R)$, (2.14)

8. Between equations (2.14) and (2.15), the I_0, K_0… should be "I_0,K_0 are Bessel's functions and C_1 and C_(2)"are constants defined by:
9. Equations (2.17) and (2.18) should be:

where I_0,K_0 are Bessel's functions and C_1 and C_(2)are constants defined by:

$$C_1=\frac{K_0(\kappa)-\zeta_r K_0(\kappa\lambda)}{I_0(\kappa\lambda)K_0(\kappa)-I_0(\kappa)K_0(\kappa\lambda)},\quad C_2=\frac{\zeta_r I_0(\kappa\lambda)-I_0(\kappa)}{I_0(\kappa\lambda)K_0(\kappa)-I_0(\kappa)K_0(\kappa\lambda)}. \tag{215}$$

Using the LT approach, analytical solution of equation (2.12) with condition (2.13) can be obtained:

$$L[U(Y,t)]=\bar{U}(Y,S)=\int_0^{\infty} U(Y,t)\exp(-St)\,dt,\quad S>0, \tag{2.16}$$

Applying the Laplace transformation of equation (2.12) on equations (2.12) and (2.13), we obtained:

$$\frac{d^2\bar{U}}{dR^2}+\frac{1}{R}\frac{d\bar{U}}{dR}-\bar{U}\left[\frac{(M^2+S)Da+1}{\gamma Da}\right]=-\frac{G[C_1 I_0(\kappa R)+C_2 K_0(\kappa R)]}{S}, \tag{2.17}$$

Subject to

$$\bar{U}(1,S)=\frac{A}{S},\quad \bar{U}(\lambda,S)=\frac{B}{S}, \tag{2.18}$$

10. Finally, equations (2.21) – (2.23) should be:

Equation (2.17) with conditions (2.18) are solved to obtain fluid velocity in terms of modified Bessel's function as:

$$\bar{U}(R,S)=C_3 I_0\left(R\sqrt{\frac{(M^2+S)Da+1}{\gamma Da}}\right)+C_4 K_0\left(R\sqrt{\frac{(M^2+S)Da+1}{\gamma Da}}\right)+\frac{GDa[C_1 I_0(\kappa R)+C_2 K_0(\kappa R)]}{S[(M^2+S)Da+1-\kappa^2]} \tag{2.19}$$

where:

$$C_3=\frac{[(M^2+S)Da+1-\kappa^2][AK_0(\lambda\delta)-BK_0(\delta)]-GDa[\zeta_r K_0(\lambda\delta)-K_0(\delta)]}{S[(M^2+S)Da+1-\kappa^2][K_0(\delta\lambda)I_0(\delta)-K_0(\delta)I_0(\delta\lambda)]}, \tag{2.20}$$

$$C_4=\frac{[(M^2+S)Da+1-\kappa^2][BI_0(\delta)-AI_0(\lambda\delta)]-GDa[I_0(\delta)-\zeta_r I_0(\lambda\delta)]}{S[(M^2+S)Da+1-\kappa^2][K_0(\delta\lambda)I_0(\delta)-K_0(\delta)I_0(\delta\lambda)]},\ \delta=\sqrt{\frac{(M^2+S)Da+1}{\gamma Da}}$$

The transient skin frictions at the outer and inner tunes are respectively obtained as follow:

$$\bar{\tau}=\left.\frac{d\bar{U}(R,S)}{dR}\right|_{R=1}=\delta[C_3 I_1(\delta)-C_4 K_1(\delta)]+\frac{GDa\kappa[C_1 I_1(\kappa)-C_2 K_1(\kappa)]}{S[(M^2+S)Da+1-\kappa^2]}, \tag{2.21}$$

$$\bar{\tau}=\left.\frac{d\bar{U}(R,S)}{dR}\right|_{R=\lambda}=\delta[C_3 I_1(\lambda\delta)-C_4 K_1(\lambda\delta)]+\frac{GDa\kappa[C_1 I_1(\lambda\kappa)-C_2 K_1(\lambda\kappa)]}{S[(M^2+S)Da+1-\kappa^2]}, \tag{2.22}$$

Also, the dimensionless transient mass flux is given by:

$$\bar{Q}=\int_1^{\lambda} R\,U(R)\,dR=\frac{C_3}{\delta}[\lambda I_1(\lambda\delta)-I_1(\delta)]-\frac{C_4}{\delta}[\lambda K_1(\lambda\delta)-K_1(\delta)]+\frac{GDa}{S[(M^2+S)Da+1-\kappa^2]_k}[C_1[\lambda I_1(\lambda\kappa)-I_1(\kappa)]-C_2[\lambda K_1(\lambda\kappa)-K_1(\kappa)]] \tag{2.23}$$

The solutions obtained for flow formation from equations (2.19 – 2.23) are in Laplace domain. Due to the complexity of the solutions, we employed the Riemann-sum approximation technique [27-29] to transform from Laplace domain to time domain. In this technique, functions in the Laplace domain, $\bar{U}(R,S)$ can be reversed to time realm by single summation:

$$U(R,t)=\frac{e^{\varepsilon' t}}{t}\left[\frac{1}{2}\bar{U}(R,\varepsilon')+Re\sum_{n=1}^{m}\bar{U}\left(R,\varepsilon'+\frac{in\pi}{t}\right)(-1)^n\right],\ 1\le R\le\lambda \tag{2.24}$$

where Re denotes to the real part of i=√(-1) , m is the number of terms used in the RSA and ε is the real part of the Bromwich contour. The RSA for the inversion involves a single summation for the numerical process. Its correctness depends on the value of ε^' and the error led by m. According to Tzou, the value of εt that best satisfied the result is 4.7 [28].

Results and Discussion

This work is dedicated to investigate the effect of electric potential, applied magnetic field and porous material on Couette flow formation of a conducting fluid in a horizontal annulus. Before establishing the role of various governing parameters, it is expedient to first check the accuracy of the solution obtained by comparing with published article in literature in the absence of externally applied electric field. Table 1 presents a numerical comparison between the present work velocity with those of Jha and Apere in the absence of electrokinetic effect (G=0)[22].

From this numerical computation, an excellent agreement is found.

Table 1: Comparison of velocity profile obtained versus those obtained by Jha and Apere [22] for M=2.0,t=5.0,λ=2.0.

	K=0		K=0	
R	Jha and Apere [22]	Present work (G=0)	Jha and Apere [22]	Present work (G=0)
1.0	0.0000	0.0000	0.0000	0.0000
1.2	0.7230	0.7230	1.9539	1.9539
1.4	1.4484	1.4484	3.1635	3.1635
1.6	2.3077	2.3077	3.9571	3.9571
1.8	3.4363	3.4363	4.5281	4.5281
2.0	5.0001	5.0001	5.0001	5.0001

To evaluate the role of governing parameters such as Debye-Hückel parameter (κ), Hartmann number (M), annular gap (λ), magnitude of electric potential (G) and dimensional time (t), we typically used the values of the physical parameters that have been utilized in previously published work in electroosomotic flows [26]. For computational purpose, in this research, 0≤κ≤10 to analyse the physical situations ranging from thin to large EDL, the zeta potentials at the walls are assumed over 0≤ζ_r≤1, and 0≤M≤5 for Hartmann number. In addition, figures with black lines signify the case where both cylinders are stationary (A=B=0), figures with red lines mean the case where the inner cylinder is moving while the outer is stationary (A=1,B=0), figures with green lines represent the case where the inner cylinder is static while the outer is in motion (A=0,B=1), and figures with blue lines mean both cylinders are moving (A=B=1).

Electric Potential

Fig. 2 depicts the dimensionless electrostatic potential in the annulus as a role of ζ. The EDL potential is found to be higher at the walls owing to the applied external voltage at the surfaces of the cylinders.

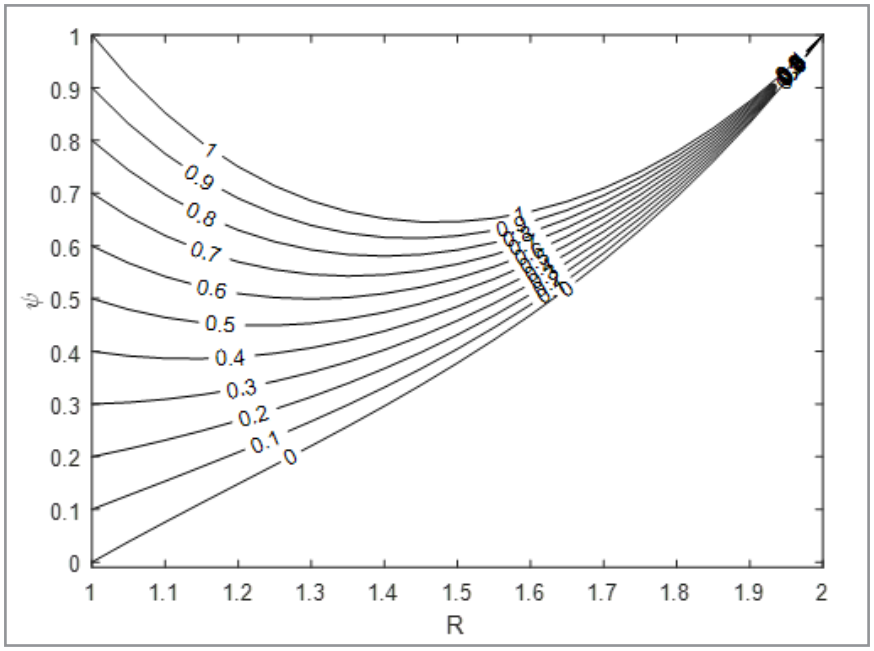

Figure 2: Electric potential for different values of ζ_r

Also, as the zeta potential at the outer surfaces of inner cylinder leaves asymmetric state, (ζ_r≠0), the electric potential in the annulus gradually changes form a linear function to a parabolic function. This scenario can be attributed to the zeta-potential supplied at the surfaces of the cylinders. Furthermore, the least electric potential is felt towards the centre of the annulus for the case of symmetric wall zeta potential.

Velocity Profile

This sub-section is devoted to presentation of velocity profile results for the current problem.

Figure 3 examines the impact of dimensionless time (t) and on velocity profile in the annulus for the cases when no motion of cylinders and at least motion of one cylinder. Fluid motion is improved by dimensionless time throughout the annulus and attain steady state solution for all cases considered. It is also obvious that the boundary layer is clearly observed for the case when both cylinders are in motion relative to other physical situations.

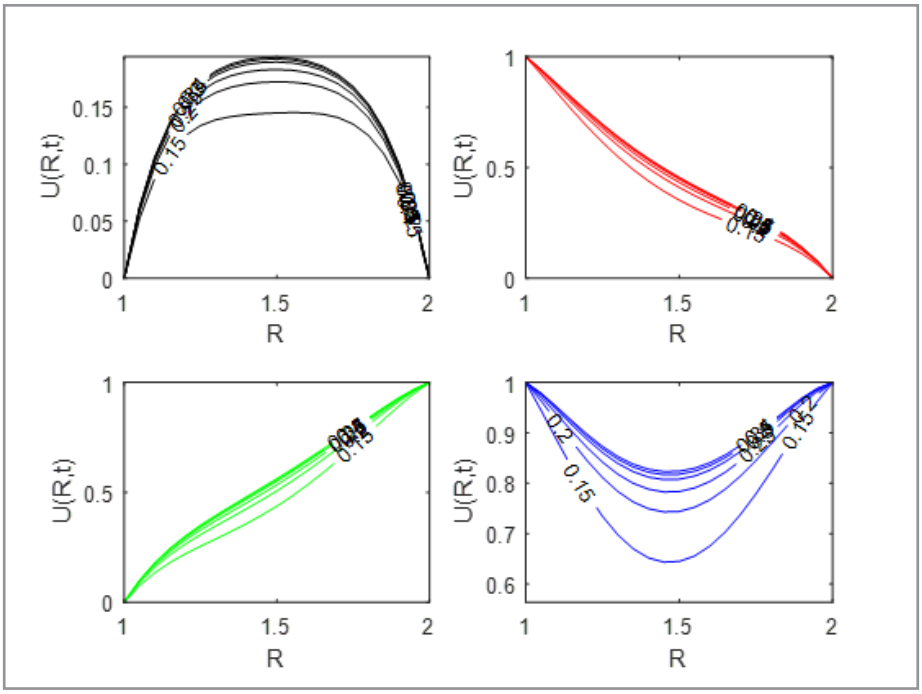

Figure 3: Velocity profile for different conditions at different time

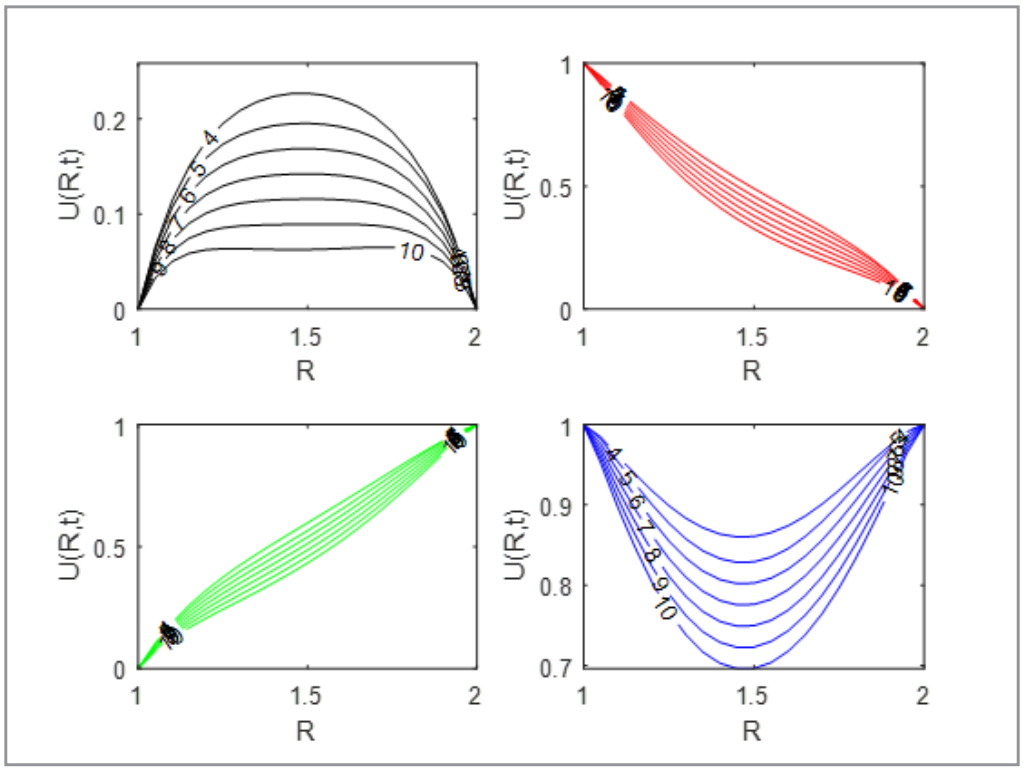

Figure 4: Velocity profile for different conditions and κ

Figure 4 shows the role of EDL size on flow formation in between the cylinders. It is found from this figure that fluid velocity decreases with increase in EDL length. This is because increasing κ, decreases the EDL length and therefore reducing the impact of the externally applied voltage gradient which should have increased the kinetic energy and hence leading to decrease in fluid velocity in the annulus. While the case of fixed boundary shows a maximum point around the middle of the boundary layer, the case when both cylinders are moves results to minimum point at the middle of the boundary layer.

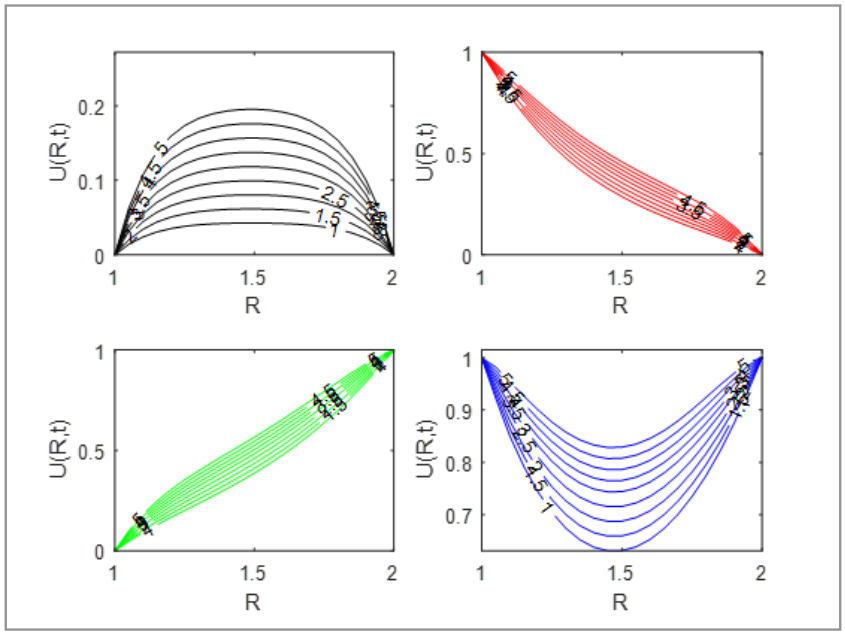

Figure 5: Velocity profile for different conditions and Da

Figure 5 illustrates the fluid velocity as a function of Darcy number (Da) for different physical situations. It is obvious from these graphs that velocity increases as Da increases regardless of the case considered. This is credited to the point that rise in magnitude of Darcy number increases the porosity of the porous material thereby increasing flow channel. Overall, fluid velocity when either of the cylinders is moving behave in the same manner.

Skin-friction

This sub-section is dedicated to investigating the impact of electrokinetic effect, Darcy number and Hartmann number on time-dependent Couette flow in a horizontal annulus filled with electrically conducing fluid. The study of shear stress continues to gain significant attention due to its engineering and technological applications, such as; high speed jets, construction of bridges and dams.

Figure 6 exhibits the joint role of magnetic field (M) and Darcy number (Da) on skin friction at the outer surface of inner cylinder in the presence of EDL. Result indicates that skin-friction increases with Da irrespective of the physical situations considered but decreases with surge in M. A careful look at the figure advises that skin friction can be reduced to nothing in the presence of very strong magnetic field (M→∞). This could be attributed to the Lorentz force acting perpendicular to flow formation which in turn retards the friction at this surface.

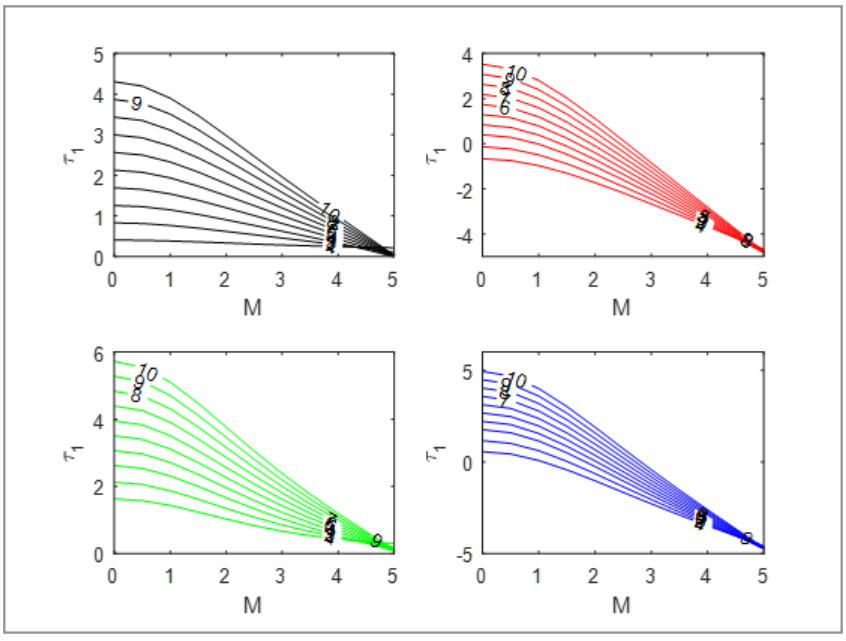

Figure 5: Skin friction for different conditions, magnetic field and Da

Figure 6 further analysed the combined impact of magnetic field and EDL size on skin friction at the outer surface of the inner cylinder for different physical situations. It is found from this figure that skin friction at the surface decreases with increase in κ for all cases considered. This is expected because rise in κ signifies a thin EDL and therefore reducing the collisions in the horizontal annulus and hence reducing the force at which the electrically conducting fluid hits the outer surface of the inner cylinder which results to lowering skin friction at the surface. A watchful look at these figures recommends that as κ,M→∞ (which corresponds to no EDL with no magnetic field), electrokinetic effect plays no role in the overall skin friction at the outer surface of inner cylinder irrespective of its magnitude. Overall, while the skin friction when the outer surface is moving and inner surface is fixed has the highest skin friction amongst the considered cases, other situations have relatively comparable values.

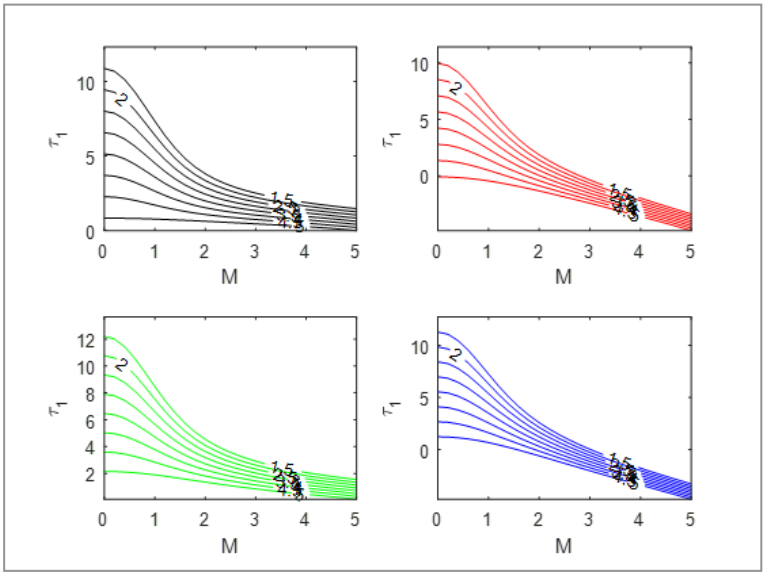

Figure 6: Skin friction for different conditions, magnetic field and κ

Mass Flow-rate

Another distinctive analysis in the study of microfluidic is the computation of the total fluid passing through the horizontal annulus in the fully developed state. Figure 7 portrays the mass flowrate for diverse values of M and κ at different time in the horizontal annulus for the case when the cylinders are either static or moving. It is observed that the amount of fluid continues to increase with κ. This may be attributed to the continuous declaration of fluid velocity caused by increasing κ. Then again, the mass flow rate is observed to be a decreasing function of Hartmann number (M). It is easy to conclude that for K=0 in the presence of strong magnetic field (M→∞), there may be stoppage of flow formation. This can be attributed to the Lorentz force acting perpendicularly to flow direction which would have been strong enough to stop flow formation as well as mass flow rate.

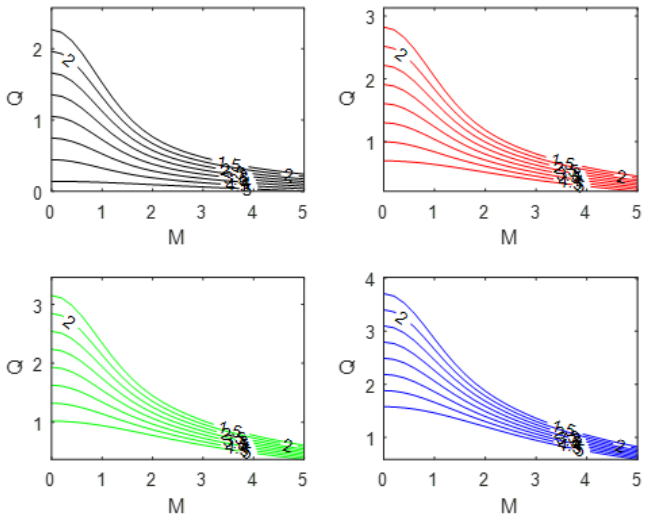

Figure 6: Mass flow rate for different conditions and κ

Figure 8 also displays the effect of Da on mass flowrate in the horizontal annulus for the case of symmetric zeta potential. It is obtained that mass flowrate increases with Da regardless of the physical situation considered. As $\kappa \to \infty$, electrokinetic influence plays no role in the overall mass flow rate regardless of the magnitude of the EDL, thereby corresponding to the results of absence of externally applied voltage (G=0). The maximum flow rate is found when both cylinders are moving relative to other physical situations.

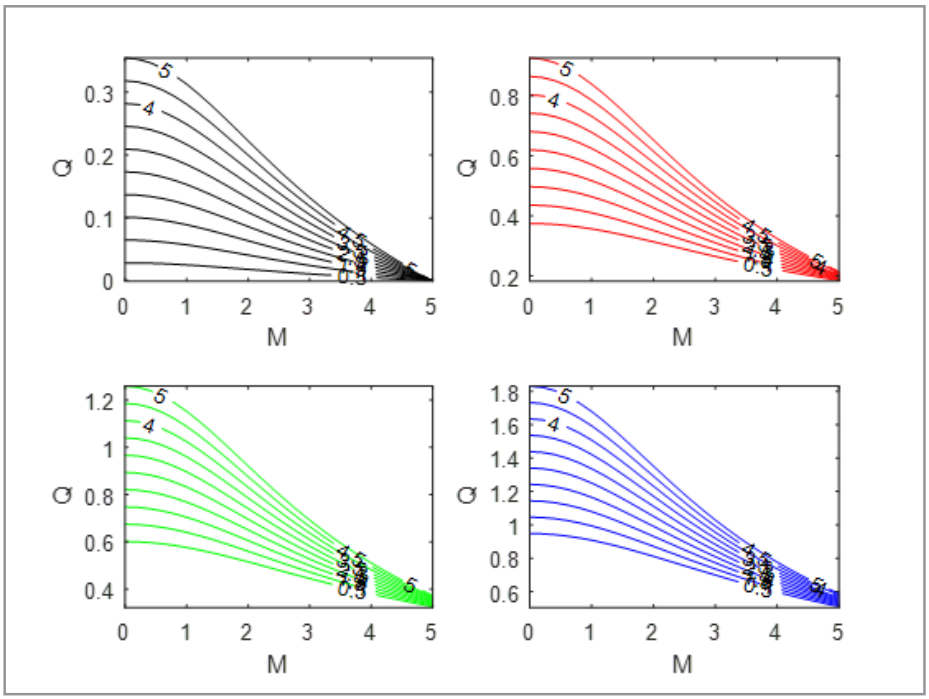

Figure 8: Mass flow rate for different conditions and Da

In general, it is found that the consideration of different moving or fixed cylinders did not distort the impact of any governing parameter on flow formation, skin friction and mass flow rate but rather acts as incrementor.

Conclusion

The time-dependent Couette flow of a conducting fluid in a horizontal annulus with combined role of electrokinetic, Darcy number and accelerated motion of outer cylinder is considered in this article. The governing equations are presented and changed to their various dimensionless forms by means of fit dimensionless parameters. Using Laplace transform technique, analytical solutions for electric field and fluid velocity are obtained. Based on the graphical represented of the obtained solutions, the subsequent inferences are drawn:

1. Velocity, mass flowrate and skin-friction decrease with increase in Debye-Hückel parameter at all-time regardless of the physical situation considered.
2. Rise in magnetic field result to corresponding decrease in fluid velocity, mass flowrate and skin friction.
3. The combined presence of strong magnetic field and Debye-Hückel parameter can lead to no flow formation and consequently zero skin-friction at the outer surface of inner cylinder.
4. Motion of the cylinders can serve as control mechanisms to lower or enhance the mass flow rate and skin friction in the flow setup.

References

1. Wall, S. (2010). The history of electrokinetic phenomena. Current Opinion in Colloid & Interface Science, 15, 119-124.
2. Karniadakis, G., Beskok, A., & Aluru, N. (2005). Microflows and Nanoflows: Fundamentals and Simulation. Springer.
3. Chang, L., Jian, Y., Buren, M., Liu, Q., & Sun, Y. (2016). Electroosmotic flow through a microtube with sinusoidal roughness. Journal of Molecular Liquids, 220, 258-264.
4. Rojas, G., Arcos, J., Peralta, M., Méndez, F., & Bautista, O. (2017). Pulsatile electroosmotic flow in a microcapillary with the slip boundary condition. Colloids and Surfaces A: Physicochemical and Engineering Aspects, 513, 57-65.
5. Probstein, R. F. (2005). Physicochemical hydrodynamics: an introduction. John Wiley & Sons.
6. Laser, D. J., & Santiago, J. G. (2004). A review of micropumps. Journal of micromechanics and microengineering, 14, R35.
7. Chakraborty, J., Ray, S., & Chakraborty, S. (2012). Role of streaming potential on pulsating mass flow rate control in combined electroosmotic and pressure-driven microfluidic devices. Electrophoresis, 33, 419-425.
8. Chakraborty, S., & Ray, S. (2008). Mass flow-rate control through time periodic electro-osmotic flows in circular microchannels. Physics of Fluids, 20, 013101.
9. Kirby, B. J., & Hasselbrink Jr, E. F. (2004). Zeta potential of microfluidic substrates: 2. Data for polymers. Electrophore-

sis, 25, 203-213.
10. Wang, C. Y., Liu, Y. H., & Chang, C. C. (2008). Analytical solution of electro-osmotic flow in a semicircular microchannel. Physics of Fluids, 20, 043603.
11. Jian, Y., Yang, L., & Liu, Q. (2010). Time periodic electro-osmotic flow through a microannulus. Physics of Fluids, 22, 013101.
12. Khaki, M., Taeibi-Rahni, M., & Ganji, D. D. (2012). Analytical solution of electro-osmotic flow in rectangular Nano-channels by combined Sine transform and MHPM. Journal of Electrostatics, 70, 451-456.
13. Arulanandam, S., & Li, D. (2000). Liquid transport in rectangular microchannels by electroosmotic pumping. Colloids and surfaces A: physicochemical and engineering aspects, 161, 89-102.
14. Katagiri, M. (1962). Flow formation in Couette motion in magnetohydrodynamics. Journal of the Physical Society of Japan, 17, 393-396.
15. Muhuri, P. (1963). Flow formation in Couette motion in magnetohydrodynamics with suction. Journal of the Physical Society of Japan, 18, 1671-1675.
16. Singh, A. K., & Kumar, N. (1983). Unsteady magnetohydrodynamic Couette flow. Wear, 89, 125-129.
17. Globe, S. (1959). Laminar Steady-State Magnetohydrodynamic Flow in an Annular Channel. The physics of fluids, 2, 404-407.
18. Jha, B. K., & Oni, M. O. (2018). Impact of mode of application of magnetic field on rate of heat transfer of rarefied gas flows in a microtube. Alexandria engineering journal, 57, 1955-1962.
19. Jha, B. K., Aina, B., & Isa, S. (2015). Fully developed MHD natural convection flow in a vertical annular microchannel: an exact solution. Journal of King Saud University-Science, 27, 253-259.
20. Jha, B. K., & Aina, B. (2016). Role of induced magnetic field on MHD natural convection flow in vertical microchannel formed by two electrically non-conducting infinite vertical parallel plates. Alexandria Engineering Journal, 55, 2087-2097.
21. Jha, B. K., & Oni, M. O. (2018). Fully developed mixed convection flow in a vertical channel with electrokinetic effects: exact solution. Multidiscipline Modeling in Materials and Structures, 14, 1031-1041.
22. Jha, B. K., & Apere, C. A. (2010). Unsteady MHD Couette flows in an annuli: the riemann-sum approximation approach. Journal of the Physical Society of Japan, 79, 1244-1247.
23. Oni, M. O., & Jha, B. K. (2023). Entropy generation analysis of electroosmotic mixed convection flow in vertical microannulus with asymmetric heat fluxes. Int. Commun. Heat Mass Transf, 145, 1068-1081.
24. Oni, M. O., & Rilwan, U. (2023). Role of suction/injection on electromagnetohydrodynamic natural convection flow in a porous microchannel with electroosmotic effect. Int. J. of Applied Mechanics and Engineering, 28, 94-113.
25. Oni, M. O., Jha, B. K. (2022). Analysis of transient buoyancy/ electroosmotic driven flow in a vertical microannulus with velocity-slip and temperature-jump. Eng. Sci. Technol, 84, 107.
26. Oni, M. O., Rilwan, U., Jha, B. K., & Jibril, H. M. (2023). Analysis of Joule heating and viscous dissipation on electromagnetohydrodynamic flow with electroosmotic effect in a porous microchannel: A heat transfer miniature enhancement. Heat Transf, 53, 989-1013.
27. Khadrawi, A. F., & Al-Nimr, M. A. (2007). Unsteady natural convection fluid flow in a vertical microchannel under the effect of the dual-phase-lag heat-conduction model. International Journal of Thermophysics, 28, 1387-1400.
28. Tzou, D. Y. (2014). Macro-to microscale heat transfer: the lagging behavior. John Wiley & Sons.
29. Jha, B. K., & Oni, M. O. (2018). Transient natural convection flow between vertical concentric cylinders heated/ cooled asymmetrically. Proceedings of the Institution of Mechanical Engineers, Part A. Journal of Power and Energy, 232, 926-939.
30. Mukhopadhyay, A., Banerjee, S., & Gupta, C. (2009). Fully developed hydrodynamic and thermal transport in combined pressure and electrokinetically driven flow in a microchannel with asymmetric boundary conditions. International Journal of Heat and Mass Transfer, 52, 2145-2154.